NASA/TM-2008-215337
NESC-RP-08-09/06-081-E

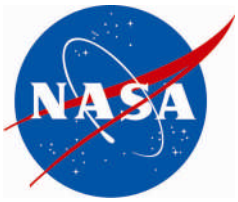

Critical Initial Flaw Size Analysis

David S. Dawicke
Analytical Services and Materials, Inc., Hampton, Virginia

Ivatury S. Raju
NASA Langley Research Center, Hampton, Virginia

Derrick J. Cheston
NASA Glenn Research Center, Cleveland, Ohio

August 2008

The NASA STI Program Office . . . in Profile

Since its founding, NASA has been dedicated to the advancement of aeronautics and space science. The NASA Scientific and Technical Information (STI) Program Office plays a key part in helping NASA maintain this important role.

The NASA STI Program Office is operated by Langley Research Center, the lead center for NASA's scientific and technical information. The NASA STI Program Office provides access to the NASA STI Database, the largest collection of aeronautical and space science STI in the world. The Program Office is also NASA's institutional mechanism for disseminating the results of its research and development activities. These results are published by NASA in the NASA STI Report Series, which includes the following report types:

- TECHNICAL PUBLICATION. Reports of completed research or a major significant phase of research that present the results of NASA programs and include extensive data or theoretical analysis. Includes compilations of significant scientific and technical data and information deemed to be of continuing reference value. NASA counterpart of peer-reviewed formal professional papers, but having less stringent limitations on manuscript length and extent of graphic presentations.

- TECHNICAL MEMORANDUM. Scientific and technical findings that are preliminary or of specialized interest, e.g., quick release reports, working papers, and bibliographies that contain minimal annotation. Does not contain extensive analysis.

- CONTRACTOR REPORT. Scientific and technical findings by NASA-sponsored contractors and grantees.

- CONFERENCE PUBLICATION. Collected papers from scientific and technical conferences, symposia, seminars, or other meetings sponsored or co-sponsored by NASA.

- SPECIAL PUBLICATION. Scientific, technical, or historical information from NASA programs, projects, and missions, often concerned with subjects having substantial public interest.

- TECHNICAL TRANSLATION. English-language translations of foreign scientific and technical material pertinent to NASA's mission.

Specialized services that complement the STI Program Office's diverse offerings include creating custom thesauri, building customized databases, organizing and publishing research results ... even providing videos.

For more information about the NASA STI Program Office, see the following:

- Access the NASA STI Program Home Page at ***http://www.sti.nasa.gov***

- E-mail your question via the Internet to help@sti.nasa.gov

- Fax your question to the NASA STI Help Desk at (301) 621-0134

- Phone the NASA STI Help Desk at (301) 621-0390

- Write to:
  NASA STI Help Desk
  NASA Center for AeroSpace Information
  7115 Standard Drive
  Hanover, MD 21076-1320

NASA/TM-2008-215337
NESC-RP-08-09/06-081-E

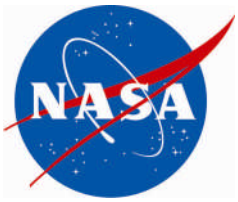

Critical Initial Flaw Size Analysis

David S. Dawicke
Analytical Services and Materials, Inc., Hampton, Virginia

Ivatury S. Raju
NASA Langley Research Center, Hampton, Virginia

Derrick J. Cheston
NASA Glenn Research Center, Cleveland, Ohio

NASA Engineering and Safety Center
Langley Research Center
Hampton, Virginia 23681-2199

August 2008

Available from:
NASA Center for AeroSpace Information (CASI)
7115 Standard Drive
Hanover, MD 21076-1320
(301) 621-0390

Critical Initial Flaw Size Analysis

D. S. Dawicke
Analytical Services and Materials, Inc.

I. S. Raju
NASA Langley Research Center

D. Cheston
NASA Glenn Research Center

Introduction

An independent assessment was conducted to determine the critical initial flaw size (CIFS) for the flange-to-skin weld in the Ares I-X Upper Stage Simulator (USS). The USS consists of several "tuna can" segments that are approximately 216 inches in diameter, 115 inches tall, and 0.5 inches thick. A 6 inch wide by 1 inch thick flange is welded to the skin and is used to fasten adjacent tuna cans. A schematic of a "tuna can" and the location of the flange-to-skin weld are shown in Figure 1. Gussets (shown in yellow in Figure 1) are welded to the skin and flange every 10 degrees around the circumference of the "tuna can". The flange-to-skin weld is a flux core butt weld with a fillet weld on the inside surface, as illustrated in Figure 2. The welding process may create loss of fusion defects in the weld that could develop into fatigue cracks and jeopardize the structural integrity of the Ares I-X vehicle. The CIFS analysis was conducted to determine the largest crack in the weld region that will not grow to failure within 4 lifetimes, as specified by NASA standard 5001 & 5019 [1].

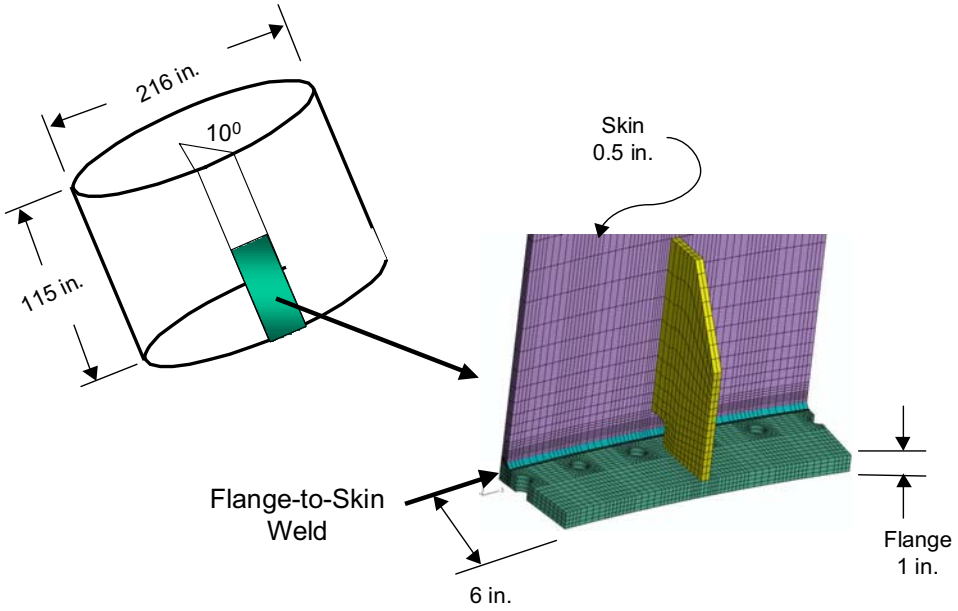

Figure 1. Schematic of an Ares I-X USS "tuna can".

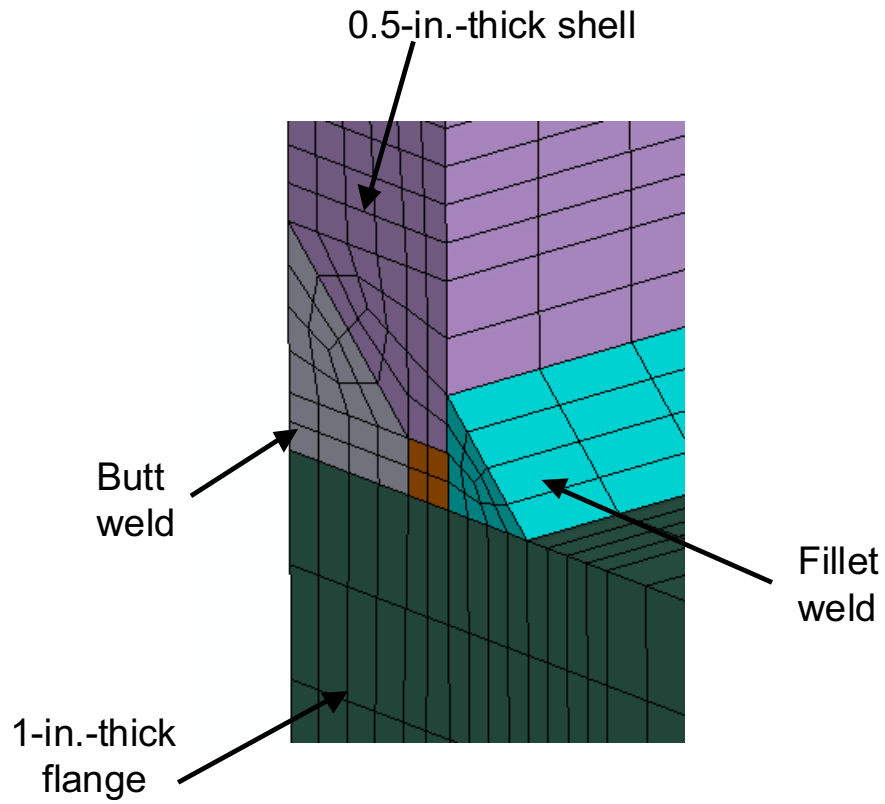

Figure 2. Schematic of the flange-to-skin weld.

A CIFS analysis assumes an initial crack size (a_i) and grows that crack according to the material behavior (fatigue crack growth rate and fracture toughness), loading spectrum for the structure, and the stress intensity factor for the crack configuration. The critical flaw size (a_{CFS}) is obtained when the maximum stress intensity factor for any one cycle of the loading spectrum exceeds the fracture toughness value. The number of spectrum repeats necessary to grow the crack from a_i to a_{CFS} is N_c. The CIFS crack length (a_{CIFS}) is defined as the largest crack length that will survive 4 repeats of the spectrum, as illustrated in Figure 3. A CIFS analysis requires the following information:

- Loading spectrum
- Stress intensity factor solution
- Material behavior that describes the fatigue crack growth rate
- Material behavior that describes the critical stress intensity factor
- A fatigue crack growth rate code

The following sections describe the definition of the loading spectrum, the stress intensity factors, the material behavior, and the fatigue crack growth analysis code. A summary section provides a review of the assumptions used in the CIFS analysis. The fatigue crack growth analysis code NASGRO [2] was used to combine all of the above information and determine the fatigue crack growth life.

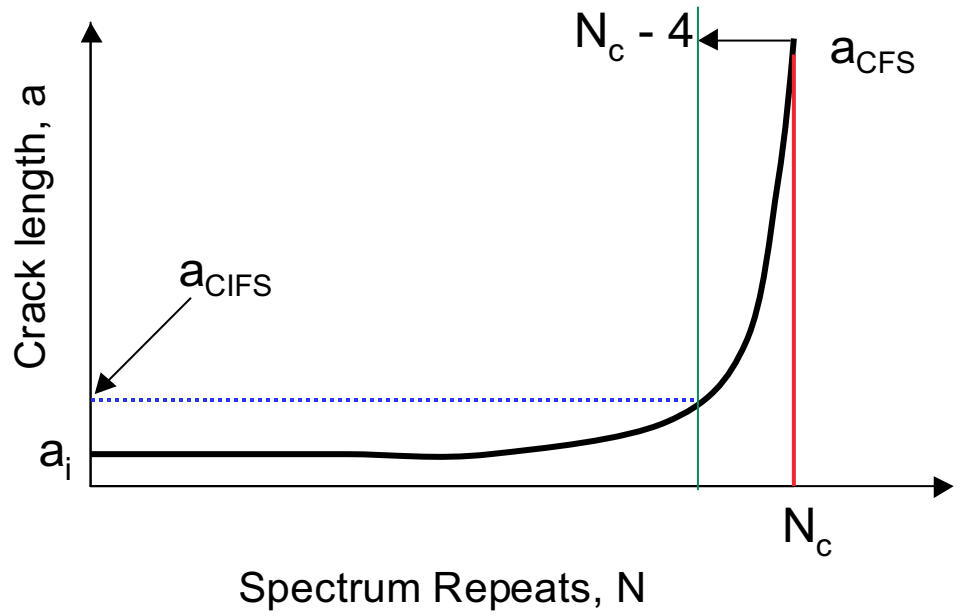

Figure 3. Schematic of the CIFS approach.

Loading Spectrum

The loading spectrum for the Ares I-X USS consists of a cyclic operational stress spectrum, a mean stress component due to the weld residual stresses, and a mean stress component due to fit-up mismatch of the mating flanges. The cyclic operational stress spectrum consists of 7 blocks: lifting, transportation, rollout, pad stay, liftoff, thrust oscillation, and ascent. Additional information on the development of the spectrum blocks is provided in Reference 3. Each block consists of one or more steps that contain pairs of maximum stress and minimum stress and the number of times (cycles) that the pair was repeated. The lifting block was estimated from the total weight of the anticipated number of "tuna cans" that would be lifted together. Three types of lifts were anticipated: 1.5 proof test, multiple segment lift, and single segment lift. The transportation block was estimated from transportation loads for the Space Shuttle External Tank. The remaining load blocks were estimated from available Ares I-X design loads, general environment, and response data. The pad stay block was modified to include a peak wind loading that was 1.7 times the nominal peak load. The resultant cyclic operational spectrum is a bounding estimate of the load magnitudes and number of cycles.

The cyclic operational spectrum was defined in terms of the number of cycles for a percentage of the peak stress. The peak stress was obtained from a finite element analysis [3] of the flange-to-skin weld with boundary conditions obtained using the maximum axial shell loads (N_x) for each block. The axial shell loads were obtained for different line load locations along the USS structure, as shown in Figure 4, and the maximum axial loads occurred at the interface of the US1 and US2 "tuna can" segments. Table 1 contains the maximum and minimum axial shell loads for each block in the spectrum. Note that a negative N_x value indicates tension and positive value compression.

The large deformation, elastic-plastic finite element analysis [4] determined the through-the-thickness axial stress distribution that resulted from the tensile axial shell load of –1,600 lb in. The calculated distribution had a stress of about 13 ksi on the inside diameter of the skin and decreased monotonically to a stress of about –0.5 ksi on the outside diameter of the skin, as shown in Figure 5. Likewise, the compressive axial shell load of 1,600 lb in was used to determine the compressive through-the-thickness axial stress distribution. The calculated distribution had a stress of about –5 ksi on the inside diameter of the skin and increased monotonically to a stress of about –3 ksi on the outside diameter.

The fit-up stresses due to a mismatch in the mating flange surfaces were calculated using a large deformation, elastic-plastic finite element analysis [4]. The worst case scenario resulted in a tensile stress of about 20 ksi on the inside diameter and tensile stress of about 3 ksi on the outside diameter, as shown in Figure 5.

The initial analysis was performed before detailed information was available for weld residual stresses and fit-up stresses. A constant through-the-thickness mean stress equal to the flow stress (54 ksi) was assumed to account for the unknown residual stresses and fit-up stresses. This assumption was believed to conservatively envelop the weld residual stresses and fit-up stresses.

The Ares I-X USS project initially proposed a balanced 6-pass weld sequence, with the last weld pass on the inner diameter (ID) of the segment skin. The actual initial weld process during the construction of the first couple of tuna can segments was a 7-pass weld sequence with the last pass on the outer diameter (OD). The weld process was changed to a 7-pass weld sequence with the last pass on the ID to minimize the tensile residual stresses on the ID for the last tuna can segments. The three weld sequences are shown in Figure 6.

The residual stresses due to the welding process were calculated from an elastic-plastic finite element analysis that took into account the heat input due to the weld process [5]. The resulting through-the-thickness distribution of residual stress was compressive on the inside diameter (ID) of the skin, became tensile in the center of the skin, and decreased to a slightly compressive value near the outside diameter (OD), for the two weld sequences that had the last pass on the ID, as shown in Figure 7. The weld sequence that had the last pass on the OD was calculated to have high tensile residual stresses on the ID and compressive residual stresses on the OD, as shown in Figure 7.

All of the CIFS analyses used the through-the-thickness distribution of the cyclic stresses and the following mean stress assumptions:

- Constant mean stress of 57 ksi – This was the initial analysis that was performed prior to obtaining information on the weld residual stresses and fit-up stresses. The value of 57 ksi was the flow stress (average of the 40 ksi yield and 74 ksi ultimate) of the material and was intended to be a conservative estimate for the influence of residual stresses and fit-up stresses.

- A mean stress that was the sum of the worst case fit-up stresses and the weld residual stresses from the 6-pass (last pass on the ID) sequence.
- A mean stress that was the sum of the worst case fit-up stresses and the tensile weld residual stresses from the 6-pass (last pass on the ID) sequence. This assumption ignores the beneficial (i.e., non-conservative) compressive residual stresses that would tend to increase the CIFS.
- A mean stress that was the sum of the worst case fit-up stresses and the weld residual stresses from the 7-pass (last pass on the ID) sequence.
- A mean stress that was the sum of the worst case fit-up stresses and the tensile weld residual stresses from the 7-pass (last pass on the ID) sequence.
- A mean stress that was the sum of the worst case fit-up stresses and the weld residual stresses from the 7-pass (last pass on the OD) sequence.
- A mean stress that was the sum of the worst case fit-up stresses and the tensile weld residual stresses from the 7-pass (last pass on the OD) sequence.

The through-the-thickness stress distributions for all analyses are summarized in Table 2. The stresses are shown as a function of the distance from the inside diameter (x).

The number of applied cycles and scaling factor for each of the 7 blocks was determined as described in Reference 3. Each block consisted of sets of the number of cyclic repeats and the minimum and maximum stresses to be applied. The minimum and maximum stresses were broken into 3 components: mean stress, axial compression stress, and axial tensile stress. The mean stress component had a minimum and maximum stress of 1 (i.e., always present during cyclic loading) and was scaled by the sum of the residual stress and fit-up stress through-the-thickness distributions given in Table 2. The axial compression component had a minimum stress of 1 and a maximum stress of 0 (i.e., only applicable at the minimum stress of the cyclic loading) and was scaled by the distribution given in Table 2. The axial tensile component had a minimum stress of 0 and a maximum stress of 1 (i.e., only applicable at the maximum stress of the cyclic loading) and was scaled by the distribution given in Table 2. The sum of the 3 minimum stress components and the 3 maximum stress components produce the cyclic applied minimum and maximum stresses. Tables 3 to 9 contain the number of cycles and the three sets of minimum and maximum stresses for the 7 blocks. The complete spectrum is obtained by applying each block once with the exception of the rollout block that was repeated 11 times to simulate 5 canceled launches, each with a return to the Vehicle Assembly Building.

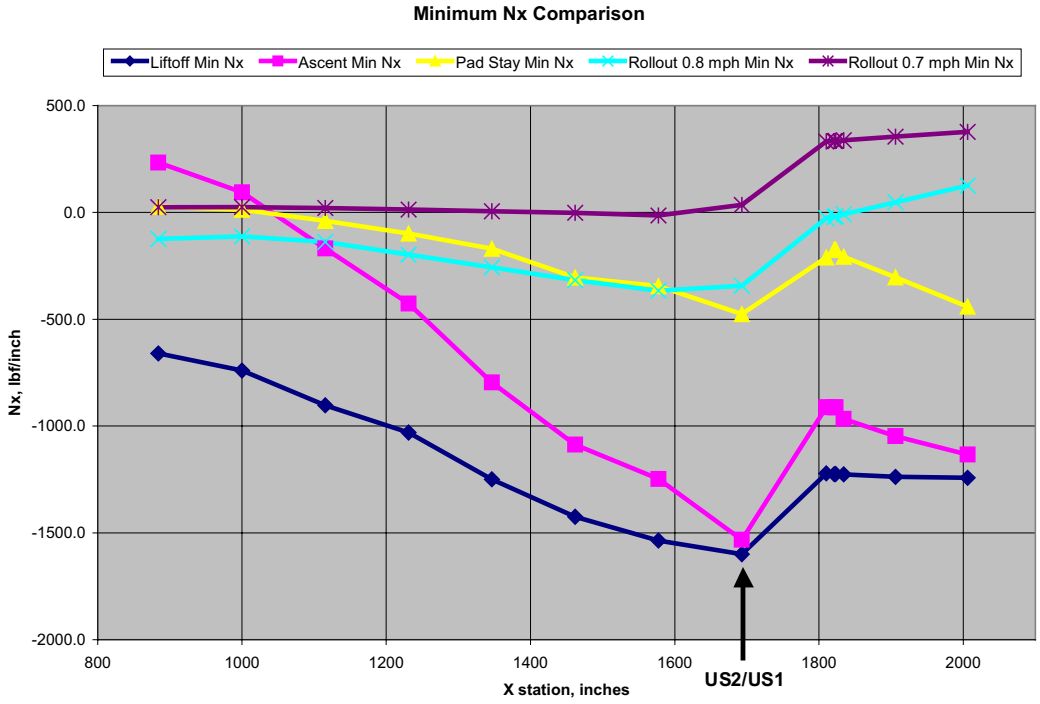

Figure 4. Maximum axial stresses (N_x) for the Ares I-X USS structure (note: negative is a positive axial load) [3].

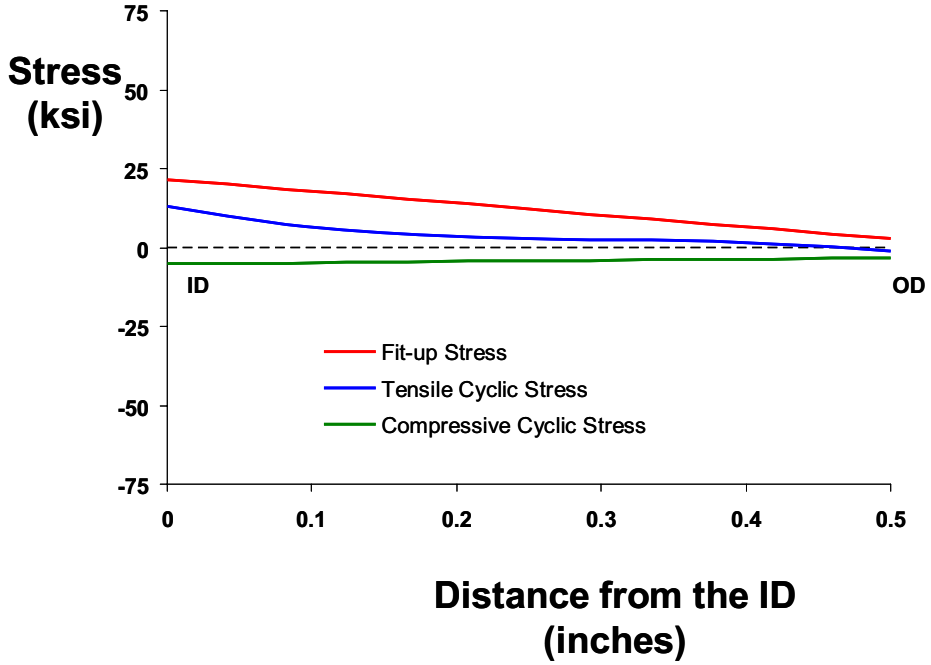

Figure 5. Fit-up stresses and cyclic stresses calculated from the elastic-plastic finite element analysis [4].

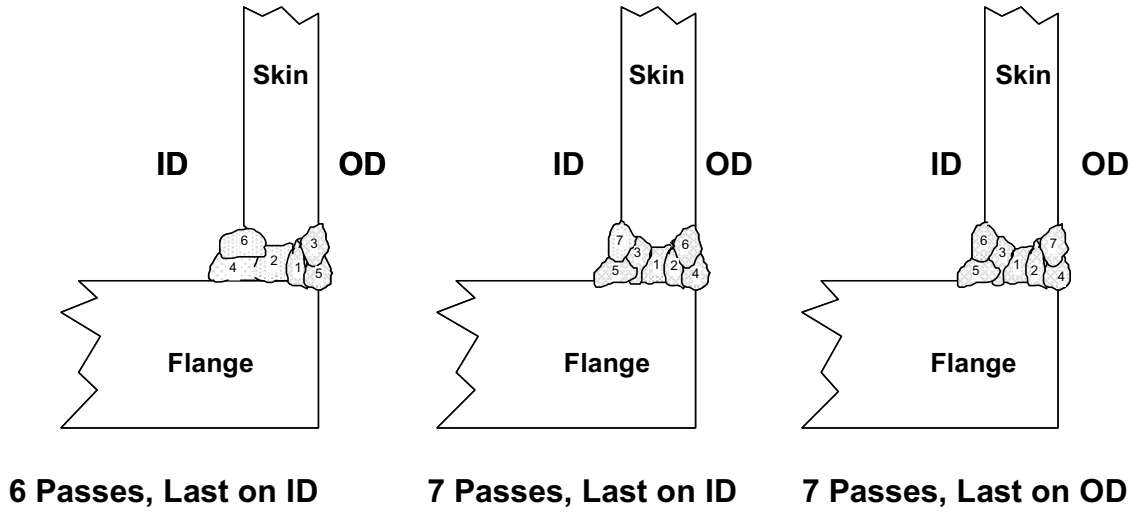

Figure 6. Schematic of the weld sequence passes used in the Ares I-X USS.

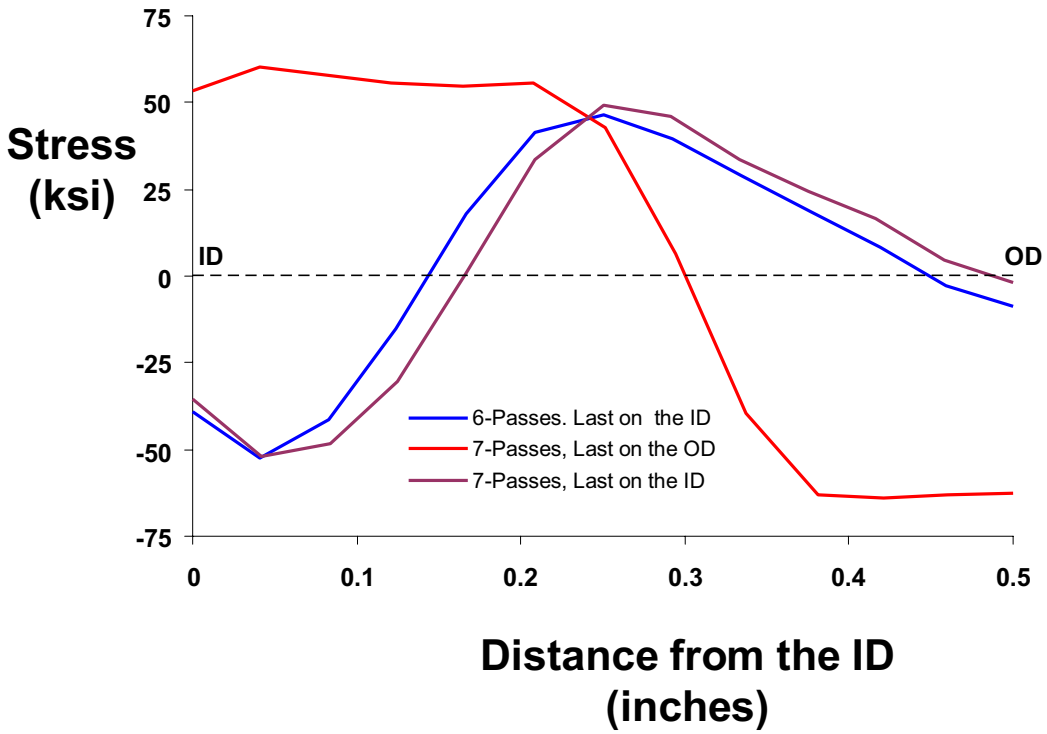

Figure 7. Weld residual stresses calculated from the elastic-plastic finite element analysis [5].

Table 1. Axial Shell Loads for the US2/US1 interface

	Max N_x (lb/in)	Min N_x (lb/in)
Lifting: Proof Load	-1092	1092
Lifting: Multi-segment	-728	728
Lifting: Single segment	-243	243
Transportation	-76	76
Rollout (0.8 mph)	-370	740
Padstay - Peak Wind	-809	1554
Padstay 100%	-476	914
Liftoff	-1600	2275
Thrust Oscillation	-120	120
Ascent	-1532	2785

Table 2
Through-the-Thickness Stress Distributions

x (inch)	Cyclic Tensile Stress (ksi)	Cyclic Compressive Stress (ksi)	6-Pass, Last on OD Stress (ksi)		x (inch)	7-Pass Last on ID Stress (ksi)		x (inch)	7-Pass Last on OD Stress (ksi)
0.000	13.26	-5.22	-39.19		0.000	53.21		0.000	-35.36
0.041	9.96	-5.06	-52.45		0.041	60.11		0.042	-51.84
0.082	7.45	-4.90	-41.58		0.080	58.04		0.083	-48.40
0.124	5.60	-4.74	-14.99		0.120	55.80		0.125	-30.34
0.166	4.32	-4.58	17.75		0.165	54.90		0.167	1.06
0.208	3.48	-4.42	41.63		0.208	55.45		0.208	33.59
0.250	2.95	-4.26	46.46		0.251	42.92		0.250	49.02
0.292	2.60	-4.10	39.36		0.294	6.45		0.292	46.22
0.335	2.29	-3.94	28.95		0.337	-39.74		0.333	33.66
0.377	1.91	-3.77	18.49		0.381	-62.97		0.375	24.26
0.419	1.31	-3.61	8.26		0.421	-64.12		0.417	16.42
0.459	0.41	-3.46	-2.63		0.460	-63.05		0.458	4.51
0.500	-0.94	-3.30	-8.73		0.500	-62.72		0.500	-1.95

Table 3
Loading Steps for the Lifting Block

Lifting Block						
	Mean Stress		Axial Compressive		Axial Tensile	
Cycles	Min Load	Max Load	Min Load	Max Load	Min Load	Max Load
42	1	1	-0.151667	0	0	0.1516667
11	1	1	-0.455	0	0	0.455
1	1	1	-0.6825	0	0	0.6825

Table 4
Loading Steps for the Transportation Block

Transportation Block						
	Mean Stress		Axial Compressive		Axial Tensile	
Cycles	Min Load	Max Load	Min Load	Max Load	Min Load	Max Load
710844	1	1	-0.002375	0	0	0.002375
142371	1	1	-0.007125	0	0	0.007125
8299	1	1	-0.011875	0	0	0.011875
1562	1	1	-0.016625	0	0	0.016625
242	1	1	-0.021375	0	0	0.021375
89	1	1	-0.026125	0	0	0.026125
17	1	1	-0.030875	0	0	0.030875
8	1	1	-0.035625	0	0	0.035625
3	1	1	-0.040375	0	0	0.040375
1	1	1	-0.045125	0	0	0.045125
1	1	1	-0.0475	0	0	0.0475

Table 5
Loading Steps for the Rollout Block

Rollout Block						
	Mean Stress		Axial Compressive		Axial Tensile	
Cycles	Min Load	Max Load	Min Load	Max Load	Min Load	Max Load
5256	1	1	-0.023125	0	0	0.0115625
10584	1	1	-0.069375	0	0	0.0346875
15768	1	1	-0.115625	0	0	0.0578125
15840	1	1	-0.161875	0	0	0.0809375
11592	1	1	-0.208125	0	0	0.1040625
9936	1	1	-0.254375	0	0	0.1271875
3744	1	1	-0.300625	0	0	0.1503125
1440	1	1	-0.346875	0	0	0.1734375
1224	1	1	-0.393125	0	0	0.1965625
576	1	1	-0.439375	0	0	0.2196875
72	1	1	-0.4625	0	0	0.23125

Table 6
Loading Steps for the Pad Stay Block

Pad Stay Block						
	Mean Stress		Axial Compressive		Axial Tensile	
Cycles	Min Load	Max Load	Min Load	Max Load	Min Load	Max Load
710844	1	1	-0.028563	0	0	0.014875
142371	1	1	-0.085688	0	0	0.044625
8299	1	1	-0.142813	0	0	0.074375
1562	1	1	-0.199938	0	0	0.104125
242	1	1	-0.257063	0	0	0.133875
89	1	1	-0.314188	0	0	0.163625
17	1	1	-0.371313	0	0	0.193375
8	1	1	-0.428438	0	0	0.223125
3	1	1	-0.485563	0	0	0.252875
1	1	1	-0.542688	0	0	0.282625
1	1	1	-0.57125	0	0	0.2975
1	1	1	-0.971125	0	0	0.50575

Table 7
Loading Steps for the Liftoff Block

Liftoff Block						
	Mean Stress		Axial Compressive		Axial Tensile	
Cycles	Min Load	Max Load	Min Load	Max Load	Min Load	Max Load
3	1	1	-0.65	0	0	0.65
2	1	1	-0.75	0	0	0.75
2	1	1	-0.85	0	0	0.85
2	1	1	-0.95	0	0	0.95
1	1	1	-1	0	0	1

Table 8
Loading Steps for the Thrust Oscillation Block

Thrust Oscillation Block						
	Mean Stress		Axial Compressive		Axial Tensile	
Cycles	Min Load	Max Load	Min Load	Max Load	Min Load	Max Load
1000	1	1	-0.075	0	0	0.075

Table 9
Loading Steps for the Ascent Block

Ascent Block						
	Mean Stress		Axial Compressive		Axial Tensile	
Cycles	Min Load	Max Load	Min Load	Max Load	Min Load	Max Load
4	1	1	-0.435156	0	0	0.239375
10	1	1	-0.609219	0	0	0.335125
8	1	1	-0.783281	0	0	0.430875
9	1	1	-0.957344	0	0	0.526625
12	1	1	-1.131406	0	0	0.622375
13	1	1	-1.305469	0	0	0.718125
8	1	1	-1.479531	0	0	0.813875
4	1	1	-1.653594	0	0	0.909625
2	1	1	-1.740625	0	0	0.9575

Stress Intensity Factor Solutions

The stress intensity factor solutions used in the Ares I-X Upper Stage Simulator (USS) flange-to-skin weld CIFS analysis were obtained from the NASGRO fatigue crack growth analysis code [2]. Two types of crack configurations were considered in the CIFS analysis: surface crack and embedded crack. The length of the crack is designated "2c" and the depth of the crack is designated "2a" for the embedded crack and "a" for the surface crack, as illustrated in the schematics shown in Figure 8.

The surface crack was idealized as a semi-elliptical crack in a flat plate using the NASGRO stress intensity factor equation SC17, as shown in Figure 9. The through-the-thickness stress distributions were accounted for using three "user defined" stress distributions to represent the mean stress, minimum cyclic stress, and maximum cyclic stress. The NASGRO code has a stress intensity factor solution for a surface crack in a

hollow cylinder subjected to axial loads (SC05), but this solution is not valid for long, shallow cracks (small ratios of a/c). The use of the flat plate stress intensity factor solution ignores the influence of the curvature of the tuna can and is a **non-conservative** assumption for long crack lengths. The extent of non-conservative stress intensity factors was estimated by comparisons of the through-the-thickness crack in a flat plate (TC01) to that of a hollow cylinder (TC08), as shown in Figure 10. This comparison assumed that the width of the flat plate was W=678 inches (the circumference of the tuna can) and the diameter of the hollow cylinder was 216 inches. The thickness of both configurations was 0.5 inches. The results indicate the difference between the two stress intensity factor solutions is small for crack lengths less than 3 inches, but was about 10% for long crack lengths.

The embedded crack was idealized as an elliptical crack in a flat plate using the NASGRO stress intensity factor equation EC02, as shown in Figure 11. The through-the-thickness stress distributions were accounted for using three "user defined" stress distributions to represent the mean stress, minimum cyclic stress, and maximum cyclic stress. As with the surface crack flat plate solution discussed above, the embedded crack flat plate solutions were also **non-conservative** relative to an embedded crack in a hollow cylinder because the influence of curvature is ignored.

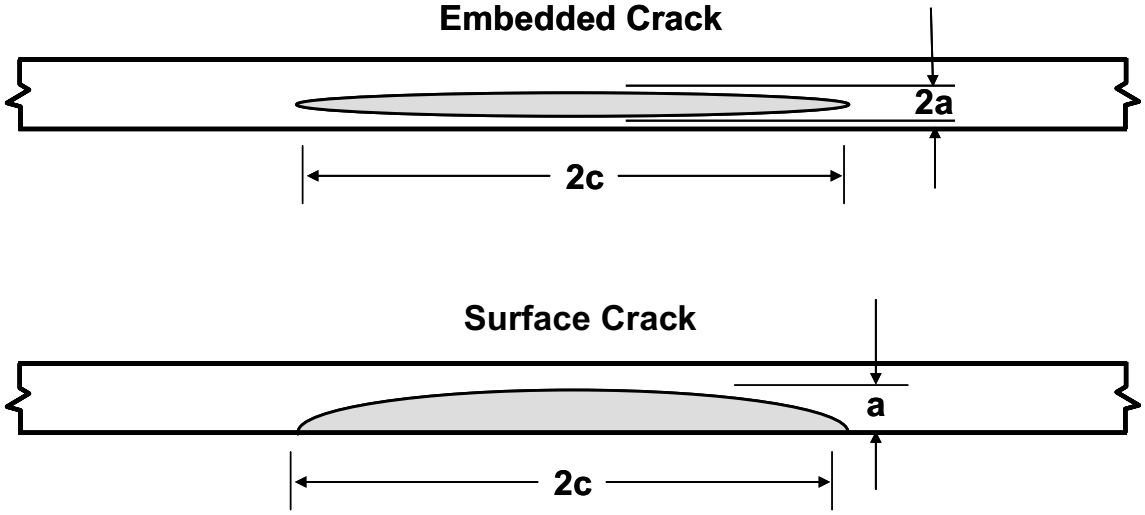

Figure 8. Schematics of the crack configurations considered in the CIFS analysis.

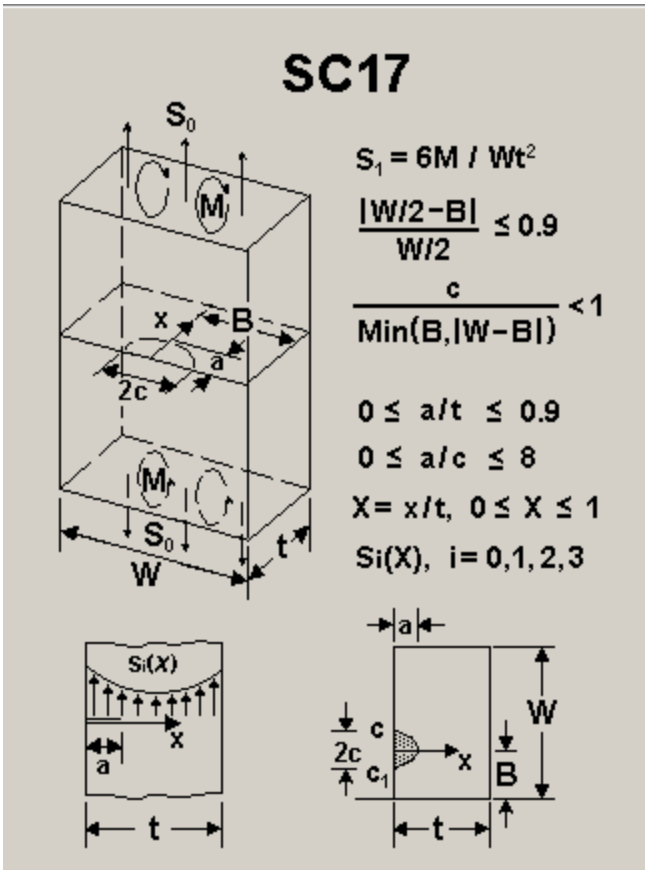

Figure 9. Illustration of the NASGRO surface crack stress intensity factor idealization [2].

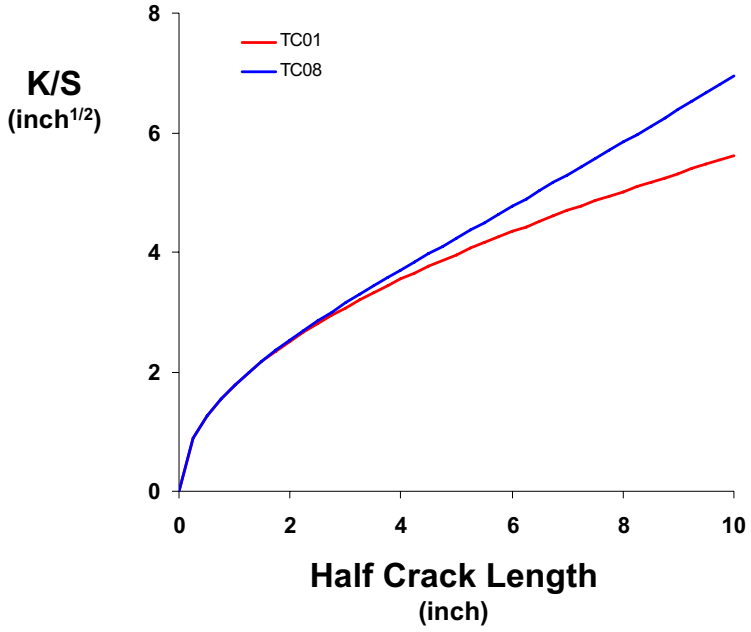

Figure 10. Stress intensity factor solution for through-the-thickness cracks in a flat plate (TC01) and in a hollow cylinder (TC08).

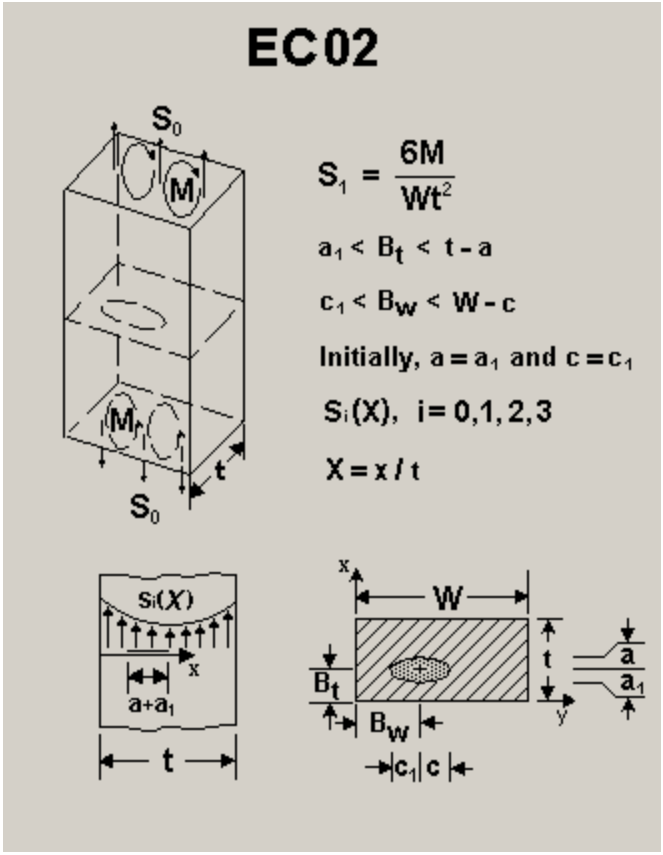

Figure 11. Illustration of the offset embedded crack stress intensity factor idealization [2].

Material Behavior

The skin and flange of the Ares I-X USS segments are made of A516 steel. The flange-to-skin weld was performed using a flux-core welding process. Tests were conducted to evaluate the material behavior of the A516 steel with particular attention to the material behavior that could be influenced by the weld process. The types of tests that were run include fatigue crack growth rate in lab air and in a salt-water environment, Charpy impact tests, and fracture tests. Parent A516 material was used for the fatigue crack growth rate tests and plates of welded material were used for the Charpy impact and fracture tests. The material behavior tests are described in Reference 6.

The NASGRO fatigue crack growth rate constants used in the CIFS analysis were:

$$\frac{da}{dN} = \frac{c\Delta K^n \left(1 - \frac{\Delta K_{th}}{\Delta K}\right)^p}{\left(1 - \frac{K_{\max}}{K_c}\right)^q} \qquad (1)$$

p = q = 0
c = 6E-10
n = 2.8

Major Assumptions

The unknowns and complexity of the USS weld required that a number of assumptions be made in order to conduct a bounding CIFS analysis. Conservative assumptions were used as much as possible to account for uncertainties in loads, material behavior, and structural configuration. The following section describes the major assumptions used in the CIFS analysis.

Fracture Toughness from the Elastic Component of J_{IC}

A516 steel is a very ductile material in the USS operational temperature range (-20°F to 190°F). This ductility allows for significant stable crack growth during the fracture process. The elastic-plastic fracture mechanics parameter J can be determined from fracture tests conducted on laboratory coupons for ductile materials. The parameter J has both elastic and plastic components, with the plastic component being dominant for ductile materials.

The value of J at the initiation of stable crack growth is defined as J_{IC}. The use of J_{IC} as a fracture mechanics parameter would neglect the beneficial contribution of the ductile stable tearing beyond the crack initiation. An additional **conservative** assumption used the elastic component of J_{IC} as the critical fracture parameter to account for the uncertainty of the similitude between laboratory coupons and surface cracks in the structural component.

Fracture Toughness Tests

Fracture tests were conducted on A516 steel with flux cored single-bevel welds. The fracture toughness values used in the CIFS analysis were obtained from the elastic component of the J_{IC} value measured in three fracture tests. The 0.1/90% lower bound value from three tests was K_c = 62 ksi inch$^{1/2}$ [6].

$$K_c = \sqrt{J_{IC_{elastic}} E} \tag{2}$$

The weld was changed to a flux cored double-bevel process after the fracture tests were conducted. The use of the single-bevel welds assumes that the fracture toughness from the double-bevel process is as high as or higher than that from the single-bevel weld. This assumption may be **unconservative**.

No Fatigue Crack Threshold

The fatigue crack growth rate behavior of many materials, including steels, has a threshold stress intensity factor range (ΔK_{th}) below which fatigue crack growth does not occur. The parameters of the NASGRO fatigue crack growth rate equation were selected to ignore any threshold effects, as shown in Figure 12. Environmental, microstructural, and loading effects can influence the fatigue crack threshold. The tests required to fully characterize the fatigue crack threshold require a great deal of time and were beyond the

scope of this assessment. Ignoring fatigue crack growth rate threshold will increase the contribution of the spectrum cycles with low cyclic stress ranges, causing the predicted crack growth rates to be faster than the actual crack growth rate. This assumption is a **conservative** assumption. The NASGRO analysis required a non-zero value of the fatigue crack growth threshold, so a value of $\Delta K_{th} = 0.001$ ksi inch$^{1/2}$ was used.

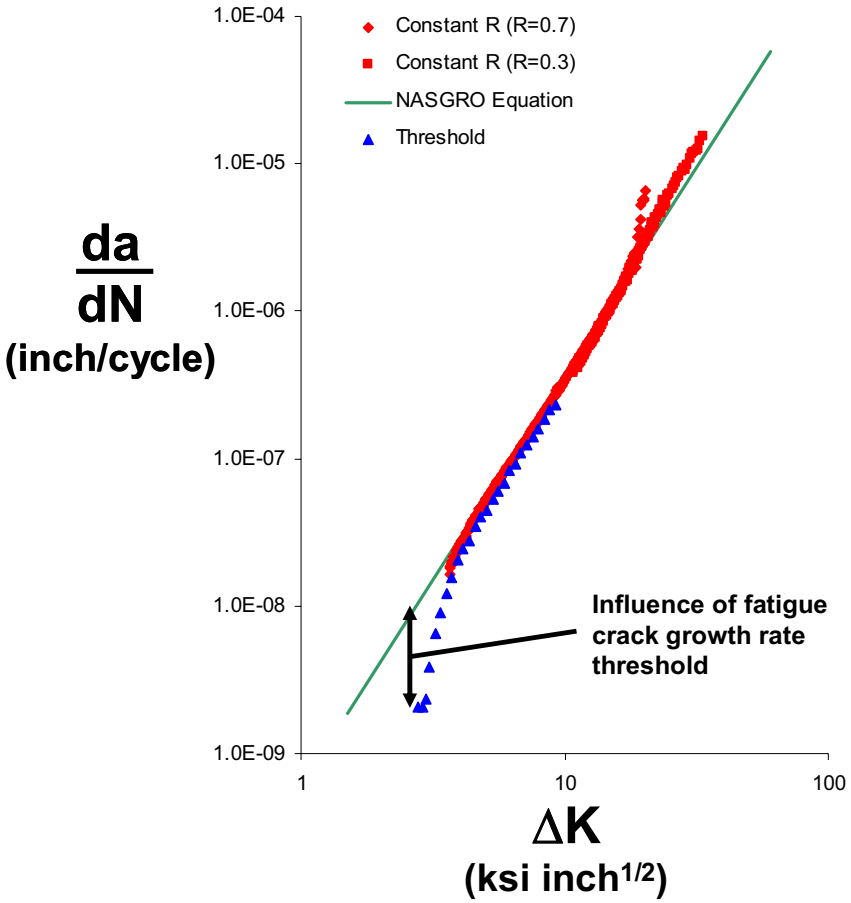

Figure 12. Influence of the threshold on the fatigue crack growth rate [6].

No Influence of Load Interaction

The fatigue crack growth rate behavior used in the CIFS analysis was based on fatigue crack growth rate tests conducted at a high stress range (R = 0.7). The NASGRO fatigue crack growth rate equation was made independent of the stress range by setting the NASGRO α parameter to a value of 5.845. This assumption makes the calculated crack growth rate behavior independent of the influence of both mean stress and load interaction. The elimination of the influence of the mean stress results in faster predicted crack growth rates for spectrum cycles with low mean stresses (**conservative assumption**). The elimination of the influence of load interaction results in the neglect of beneficial fatigue crack retardation due to high overloads (**conservative assumption**) and the neglect of damaging fatigue crack acceleration due to high underloads **(non-conservative assumption**). The makeup of the loads in the USS spectrum suggests that the retardation effects would be much greater than the acceleration effects.

Location of Crack and Stress Distribution

An elastic-plastic, large deformation finite element analysis [4] was conducted to determine the stresses in the USS structure. The USS structure is subjected to axial loads and moments, resulting in a distribution of shell loads (N_x) around the circumference of the structure, as illustrated in Figure 13. The finite element analysis assumed that the shell loads were constant around the circumference ($\tilde{N}_x$) and equal to the peak value (**conservative assumption**). The resulting axial stress along the weld oscillated around the circumference of the structure due to local influence of bolt holes and gussets. The CIFS analysis assumed that the crack started at the peak stress location and that the stress at this location was constant around the circumference of the structure (**conservative assumption**).

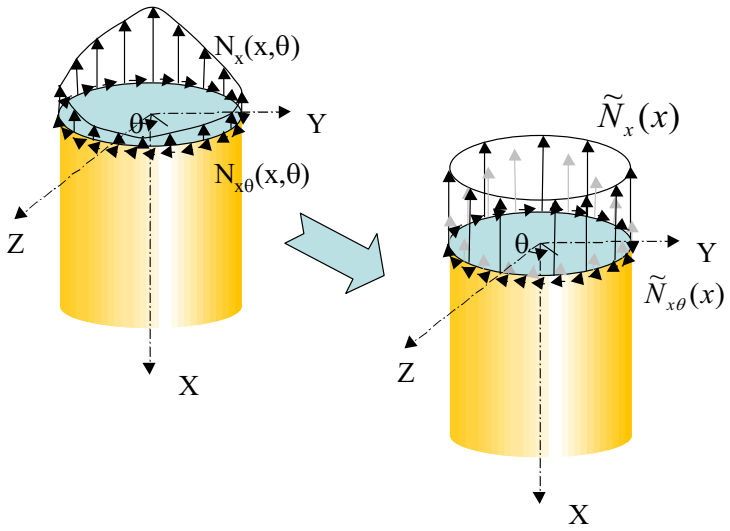

Figure 13. Illustration of the shell loads used in the finite element analysis [4].

Cyclic Tensile and Compressive Loads

The elastic-plastic finite element analysis [4] calculated stresses due to both the tensile and compressive components of the shell loads. The locations of the peak tensile and peak compressive loads were at different points along the circumference of the structure. The CIFS analysis assumed that the peak tensile and peak compressive loads occurred at the same location, increasing the applied stress range (**conservative assumption**).

Behavior of the Weld Material

The elastic-plastic finite element analysis assumed that the material response (i.e., elastic modulus and yield behavior) of the weld material is the same as the behavior of the parent material. The testing of the material response of the weld material was beyond the scope of this assessment. This assumption could result in **conservative or non-conservative** results.

Weld Residual Stresses

An elastic-plastic finite element analysis [5] was used to calculate the weld residual stresses using weld process parameters. The analysis assumed a crack-free weld and generated a through-the-thickness distribution of residual stress around the circumference of the structure. The peak residual stress was used as a mean stress in the CIFS analysis and the peak distribution was assumed to be constant around the circumference of the structure (**conservative assumption**). The CIFS analysis assumed that the through-the-thickness distribution in residual stress remained constant after the introduction of a crack and remained constant as the crack grew. This assumption could result in **conservative or non-conservative** results.

Linear Elastic Fracture Mechanics (LEFM)

The CIFS analysis assumed that LEFM assumptions apply for the USS load spectrum and material. The residual stresses that develop due to the welding process may elevate the mean stress to near yield levels. The cyclic spectrum that results from the sum of the cyclic and mean stresses could result in local yielding along the weld. However, after the initial yielding, the subsequent cycles will load and unload elastically as illustrated in Figure 14. The CIFS analysis assumes that LEFM conditions apply after the initial yielding. This assumption could result in **conservative or non-conservative** results.

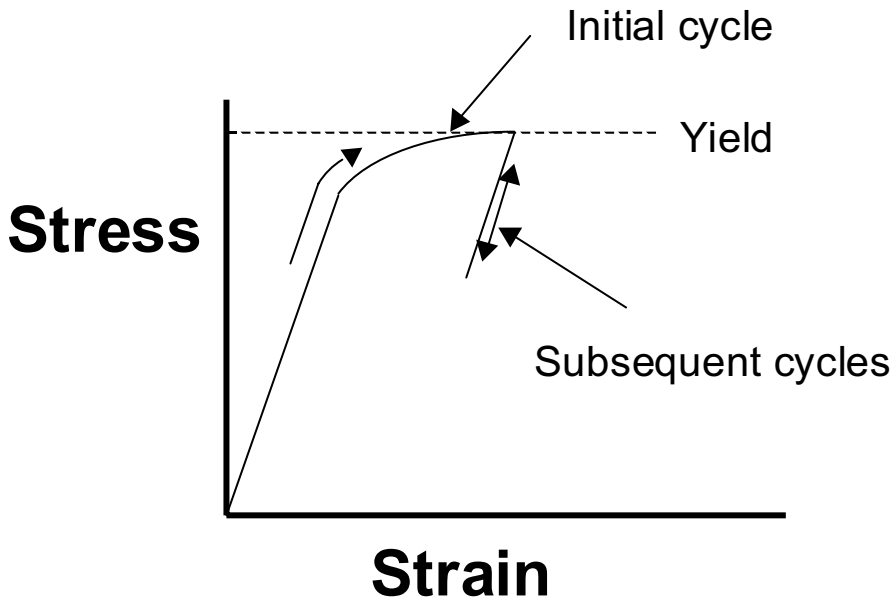

Figure 14. Illustration of elastic cyclic loading after initial yielding.

Fit-up Stresses

An elastic-plastic finite element analysis [4] was conducted to evaluate the influence of mismatch of the mating flange surfaces on the stresses along the weld. These fit-up stresses would elevate the mean stresses in the same manner as the weld residual stresses. A number of mismatch scenarios were examined and the CIFS analysis was conducted using the case with the largest weld region stresses (**conservative assumption**).

CIFS Results

The critical initial flaw size (CIFS) analyses were conducted using the NASGRO fatigue life code [2]. The analysis considered long surface and embedded cracks and determined the combination of crack length and depth that would grow to a critical value in 4 repeats of the spectrum. A plot of the critical crack depth as a function of the critical crack length will indicate the safe and non-safe combinations of crack length and depth, as shown in Figure 15.

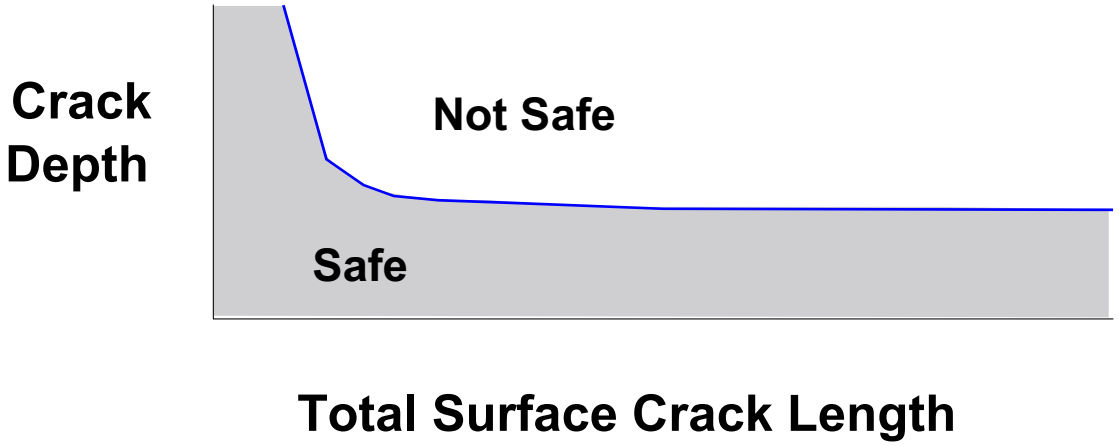

Figure 15. Schematic of the CIFS results

Cracks in a welded structure typically initiate from surface or sub-surface defects. Surface defects could occur at the inside surface (ID) or the outside surface (OD). Sub-surface defects could occur anywhere in the interior of the weld. A fatigue crack that starts as a surface crack will transition to a through-the-thickness crack when the stress intensity factor at the maximum depth location reaches a critical value. A fatigue crack that starts as an embedded crack will transition to a surface crack when the stress intensity factor at one of the depth locations reaches a critical value. This CIFS analysis assumes that any through-the-thickness crack will be critical after the transition from surface or embedded crack. The stress intensity factor (both in the length and depth directions) for an embedded crack is less than that for surface cracks. Thus, the surface crack CIFS would provide a lower bound for all similar sized embedded cracks, as shown in Figure 16.

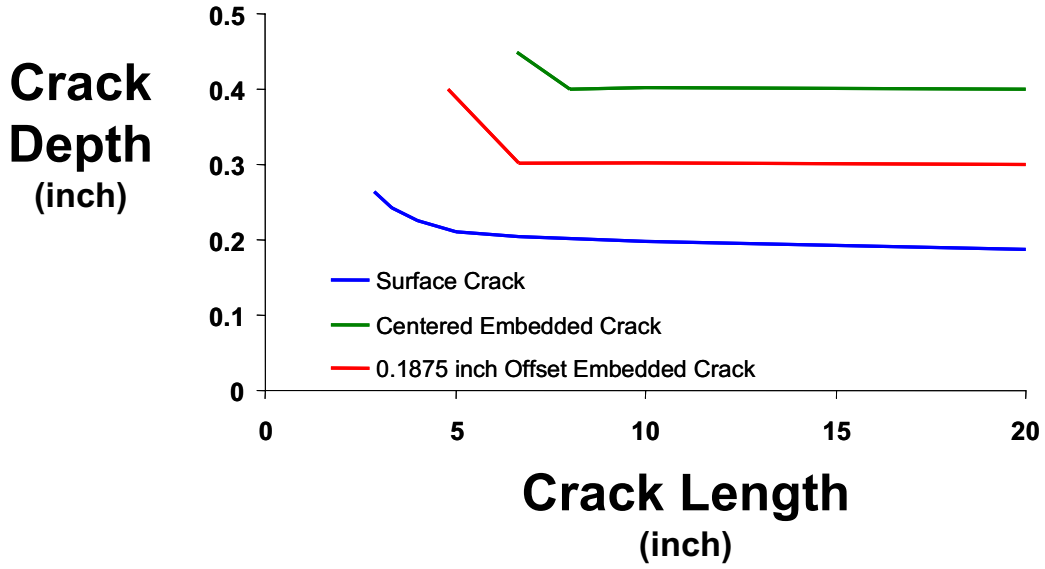

Figure 16. Schematic of the CIFS results

The stress intensity factor that drives the crack growth is calculated from the crack shape (length and depth), crack location, and the loading conditions (mean and cyclic stresses). The two components of the mean stress (weld residual stresses and fit-up stresses) and the axial cyclic stresses are not symmetric about the mid-thickness of the material, thus the stress intensity factor for a crack of a given shape and size will be different depending on the through-the-thickness location of the crack. The fit-up stresses and the axial cyclic stresses both have the peak tensile stress on the ID surface. The weld residual stresses for the 7-pass weld sequence with the last pass on the OD also has a peak tensile stress on the ID surface, resulting in a lower CIFS for cracks initiating on the ID surface than for cracks initiating on the OD surface, as shown in Figure 17. The compressive weld residual stresses inhibited any crack growth for cracks initiated on the OD surface. Neglecting the compressive weld residual stresses in the analyses (denoted "Pos RS Only" in Figure 17) did not show an influence of the CIFS behavior of the ID cracks because of the dominate tensile weld residual stresses on the ID surface, but did predict a decrease in the CIFS for the cracks that initiate on the OD surface.

The CIFS analysis that used a constant mean stress of 54 ksi to represent the weld residual stresses and the fit-up stresses predicted a smaller CIFS for cracks that initiate on the ID surface than for cracks that initiate on the OD surface, as shown in Figure 18. The difference in the CIFS for ID and OD cracks was relatively small because the difference in through-the-thickness cyclic stress was relatively small compared to the magnitude of the mean stress. Likewise, for the CIFS analysis of the 6-pass weld sequence with the last pass on the ID, the difference between the CIFS for ID and OD cracks was also relatively small, as shown in Figure 19. However, in this case the similarity in behavior was based on the dominance of the high tensile residual stresses in the mid-thickness region. The CIFS for cracks on the ID was reduced if the compressive residual stresses were ignored, but the CIFS for the cracks on the OD was not influenced by neglecting the compressive residual stresses. The CIFS analysis for the 7-pass weld sequence with the

last pass on the ID was similar to the behavior of the 6-pass weld sequence with the last pass on the OD, except the CIFS for the OD crack was slightly lower, as shown in Figure 20.

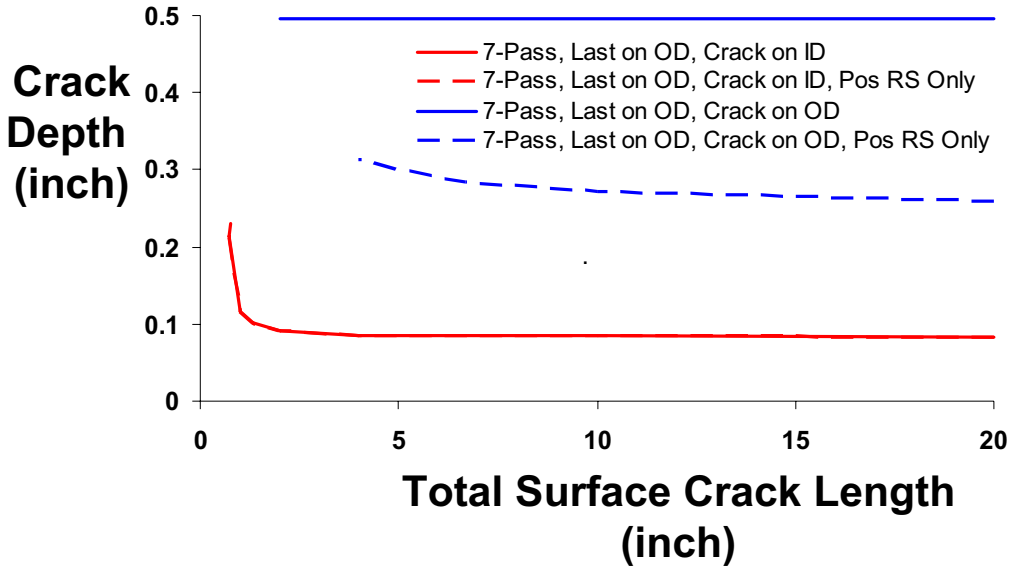

Figure 17. CIFS results for the 7-pass weld sequence with the last pass on the OD.

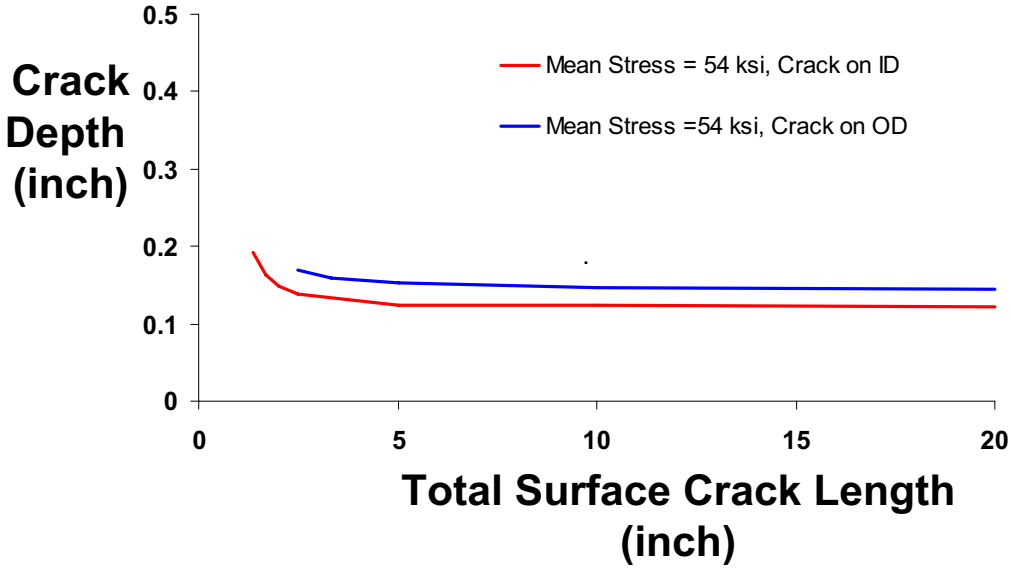

Figure 18. CIFS results for the constant 54 ksi mean stress analysis.

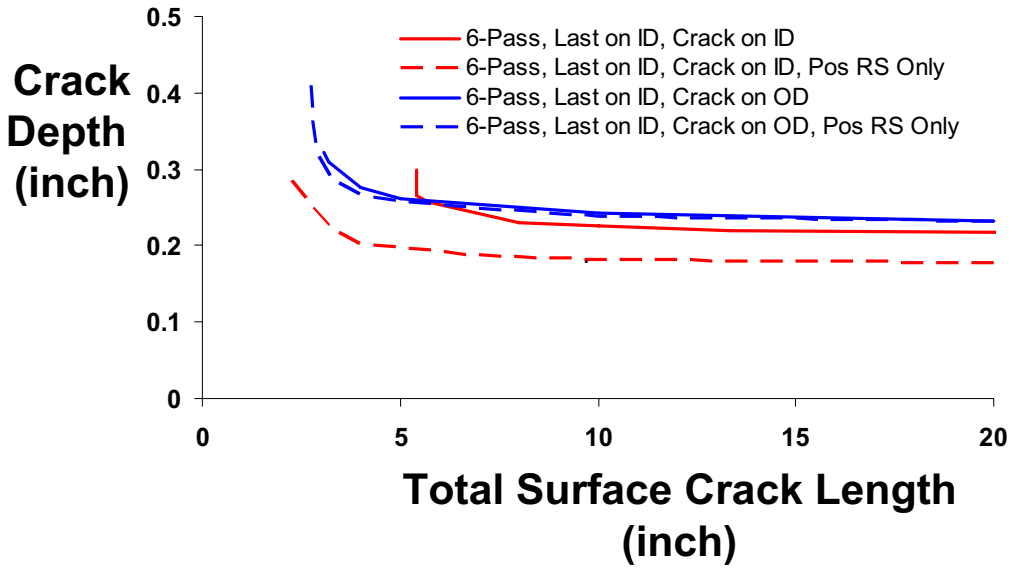

Figure 19. CIFS results for the 6-pass weld sequence with the last pass on the ID.

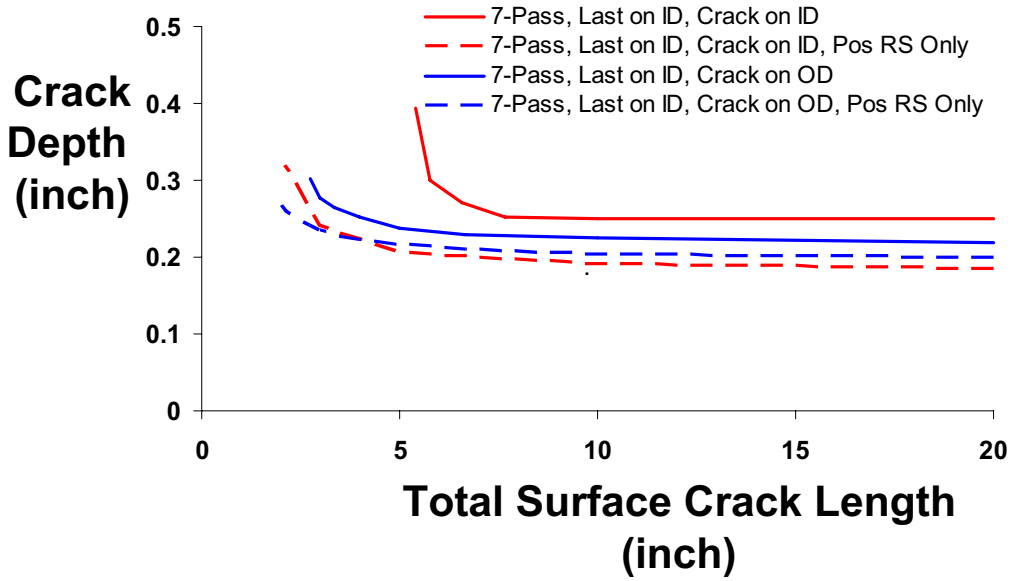

Figure 20. CIFS results for the 7-pass weld sequence with the last pass on the ID.

Crack Growth Damage by Spectrum Block

The crack growth damage accumulated for the seven different spectrum blocks was characterized using the ID surface crack configuration and the following conditions: fracture toughness of 62. ksi inch$^{1/2}$, 6-pass (last pass on ID) residual stress distribution, and the worst case fit-up stresses. Each set of applied loading cycles in a spectrum block is represented by the stress range (ΔS) and the number of applied cycles, as shown in Figure 21. The crack growth rate damage was accumulated for each set of applied cycles and plotted as symbols for damage that exceeds 20%, 15%, 10%, and 5% of the total crack growth rate damage. All of the sets of loading cycles that exceeded 5% of the total crack growth rate damage were in the rollout spectrum block. The rollout spectrum block

accounted for 96% of the crack growth damage, as shown in Figure 22. The pad stay and ascent blocks accounted for 3% and 1% of the total damage, respectively. Note that the peak stress that governs the CFS occurs in the liftoff segment, but this segment contains less than 1% of the total crack growth rate damage due to the limited number of cycles that are present in the block.

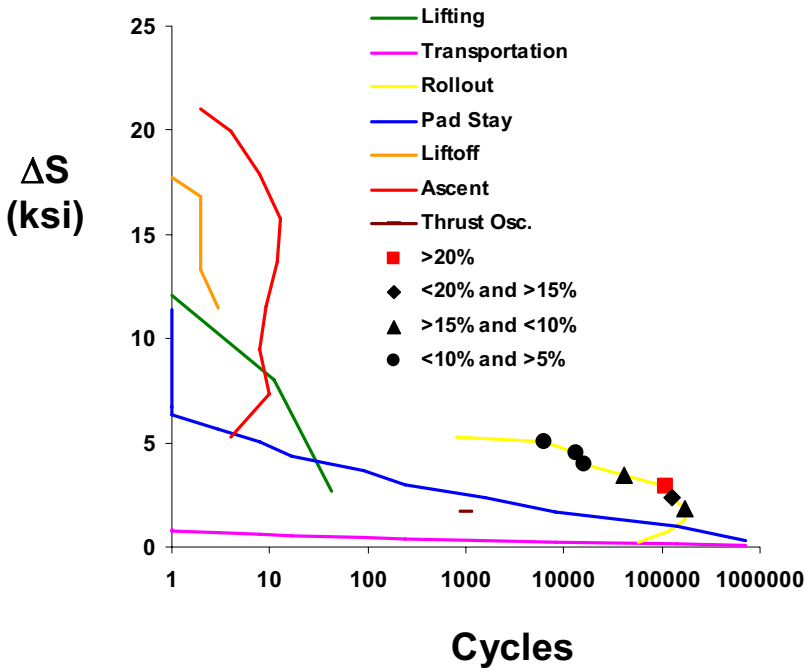

Figure 21. Crack growth damage for sets of applied loading cycles for each spectrum block.

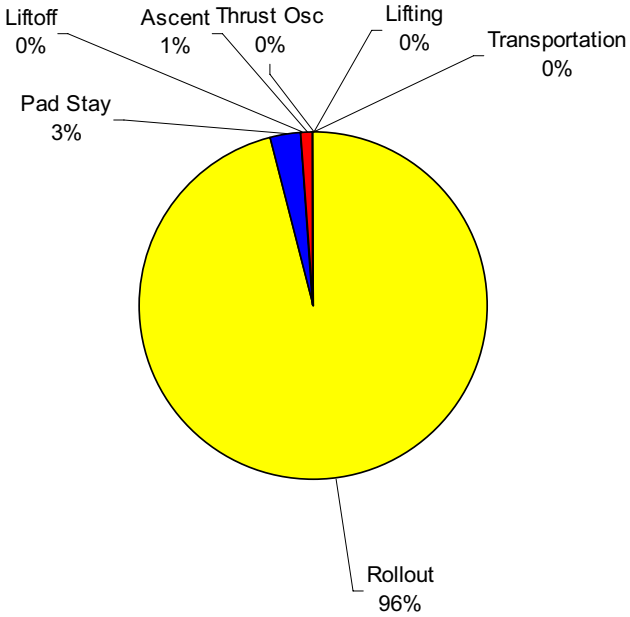

Figure 22. Crack growth damage for each spectrum block.

Summary

A critical initial flaw size (CIFS) analysis was conducted on the flange-to-skin weld of the Ares I-X Upper Stage Simulator. The analysis used linear elastic fracture mechanics assumptions to predict the fatigue crack growth rate of surface and embedded cracks in the inside (ID) and outside (OD) surfaces of the weld. The analyses used a number of assumptions, the majority of which were very conservative, to account for the unknowns and uncertainties of the problem. The non-conservative assumptions were considered to be small relative to the conservative assumptions. The analyses considered four different mean stress assumptions to account for the weld residual stresses and fit-up stresses:

- Constant mean stress of the flow stress (54 ksi) to account for the weld residual stresses and fit-up stresses
- Residual stresses calculated from a 6-pass weld sequence with the last pass on the ID and the worst case fit-up stresses
- Residual stresses calculated from a 7-pass weld sequence with the last pass on the ID and the worst case fit-up stresses
- Residual stresses calculated from a 7-pass weld sequence with the last pass on the OD and the worst case fit-up stresses

The CIFS results for each of the mean stress assumptions are shown in Figure 23. The assumption of the mean stress equal to the flow stress (54 ksi) provided the lowest bound on the CIFS for all cases except for ID cracks in the 7-pass weld sequence with the last pass on the OD. The 7-pass weld sequence with the last pass on the OD results in high tensile residual stresses on the ID surface. This is the same location that experiences the peak fit-up and cyclic stresses. Neglecting the compressive components of the weld residual stresses had no influence on the CIFS for 5 of the 8 combinations of crack location and mean stress assumption and provided a lower CIFS for the other 3 combinations.

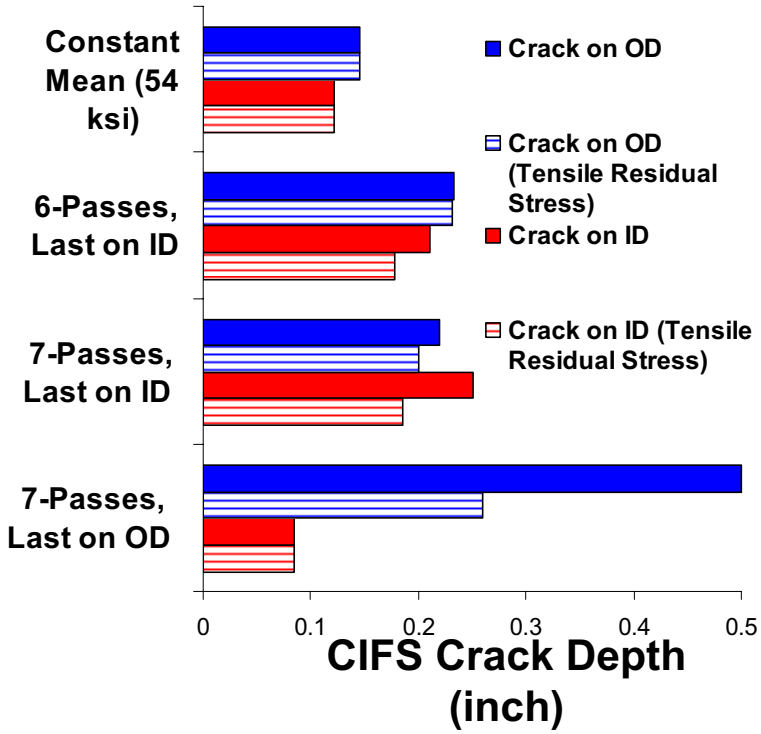

Figure 23. Summary of the CIFS results.

References

1. NASA-STD-5001A & NASA-STD 5019
2. NASGRO User's Guide.
3. Larsen, C., "Ares I-X USS Fracture Analysis Loads Spectra Development", NASA/TM-2008-215335.
4. Knight, N., Phillips, D., and Raju, I. S., "Ares I-X USS Stress Analysis", NASA/TM-2008-215336.
5. Brust, F., "Ares I-X USS Weld Residual Stress Analysis", NASA/TM-2008-215339.
6. Dawicke, D. S., S. A. Smith, and I. S. Raju "Ares I-X USS Material Testing", NASA/TM-2008-215338.

REPORT DOCUMENTATION PAGE

Form Approved
OMB No. 0704-0188

1. REPORT DATE *(DD-MM-YYYY)*	2. REPORT TYPE	3. DATES COVERED *(From - To)*
01-08-2008	Technical Memorandum	December 2006 - January 2008

4. TITLE AND SUBTITLE

Critical Initial Flaw Size Analysis

5a. CONTRACT NUMBER

5b. GRANT NUMBER

5c. PROGRAM ELEMENT NUMBER

6. AUTHOR(S)

Dawicke, David S., Raju, Ivatury S., Cheston, Derrick J.

5d. PROJECT NUMBER

5e. TASK NUMBER

5f. WORK UNIT NUMBER

510505.03.07.01.11

7. PERFORMING ORGANIZATION NAME(S) AND ADDRESS(ES)

NASA Engineering and Safety Center
Langley Research Center
Hampton, VA 23681-2199

8. PERFORMING ORGANIZATION REPORT NUMBER

L-19516 NESC-RP-08-09/06-081-E

9. SPONSORING/MONITORING AGENCY NAME(S) AND ADDRESS(ES)

National Aeronautics and Space Administration
Washington, DC 20546-0001

10. SPONSORING/MONITOR'S ACRONYM(S)

NASA

11. SPONSORING/MONITORING REPORT NUMBER

NASA/TM-2008-215337

12. DISTRIBUTION/AVAILABILITY STATEMENT

Unclassified-Unlimited/Publicly Available
Subject Category 39 - Structural Mechanics

13. SUPPLEMENTARY NOTES

14. ABSTRACT

An independent assessment was conducted to determine the critical initial flaw size (CIFS) for the flange-to-skin weld in the Ares I-X Upper Stage Simulator (USS).

15. SUBJECT TERMS

NESC, CIFS, flange-to-skin weld, Loading Spectrum

16. SECURITY CLASSIFICATION OF:			17. LIMITATION OF ABSTRACT	18. NUMBER OF PAGES	19a. NAME OF RESPONSIBLE PERSON
a. REPORT	b. ABSTRACT	c. THIS PAGE			STI Help Desk (email: help@sti.nasa.gov)
UU	UU	UU	UU	30	19b. TELEPHONE NUMBER *(Include area code)* (301) 621-0390